REVIEW ARTICLES | INSIGHT
PUBLISHED ONLINE: 20 DECEMBER 2016 | DOI: 10.1038/NMAT4778
nature materials

Materials for solar fuels and chemicals

Joseph H. Montoya[1,2†], Linsey C. Seitz[1,2†], Pongkarn Chakthranont[1,2], Aleksandra Vojvodic[1,2], Thomas F. Jaramillo[1,2] and Jens K. Nørskov[1,2*]

The conversion of sunlight into fuels and chemicals is an attractive prospect for the storage of renewable energy, and photoelectrocatalytic technologies represent a pathway by which solar fuels might be realized. However, there are numerous scientific challenges in developing these technologies. These include finding suitable materials for the absorption of incident photons, developing more efficient catalysts for both water splitting and the production of fuels, and understanding how interfaces between catalysts, photoabsorbers and electrolytes can be designed to minimize losses and resist degradation. In this Review, we highlight recent milestones in these areas and some key scientific challenges remaining between the current state of the art and a technology that can effectively convert sunlight into fuels and chemicals.

As CO_2 levels in the atmosphere increase and it becomes clear that this has substantial consequences for our climate, developing alternatives to fossil fuels is more urgent than ever. Fuels are unrivalled for energy storage and we have an enormous infrastructure built to handle fuels for transportation and heating. In addition, the chemical industry and all the products and materials that we rely on in modern society are completely reliant on fossil feedstocks. This motivates the development of sustainable processes to generate fuels and chemical feedstocks from water and CO_2 using solar energy; such a process is analogous to photosynthesis in nature and is sometimes referred to as artificial photosynthesis. There are large scientific and technical challenges involved in making even the simplest fuel, H_2, and even more so for carbon-based fuels by means of CO_2 reduction. Here we describe some of the recent progress and the obstacles that need to be surmounted to find economically viable solutions. In accordance with the theme of materials for sustainable energy, we focus on solid state devices for the production of solar fuels. There have also been important developments in molecular catalysis for fuels and we refer the interested reader to a recent review[1].

Electrochemical water splitting or CO_2 reduction powered by a renewable energy source such as the sun can be achieved using various device configurations. One such configuration is to connect a photovoltaic (PV) to a separate electrolyser with catalysts that drive the necessary conversion reactions; this design is known as PV/electrolysis and is illustrated in Fig. 1a. Another possibility is to combine these two pieces into a fully integrated system where the catalyst is deposited directly on top of the solar absorbers to create a photoelectrochemical (PEC) device (Fig. 1b). A range of intermediate configurations also exists that allow partial decoupling of the device components and set various benefits and constraints on the device operation.

In either scheme, solar-driven electrochemical water splitting devices are more developed than those for CO_2 reduction, as the hydrogen evolution reaction (HER) for water splitting is far less complex than the CO_2 reduction reaction (CO_2RR).

Both PV/electrolysis and PEC devices require photon absorbers that can harvest solar energy efficiently. They also need catalysts for water splitting and for fuel production. In addition, PEC devices require effective integration of the photon absorber and the catalyst. Here we will address each of these challenges: photon capture, electrocatalysis and integration. We begin with a discussion of some critical techno-economic aspects of solar-to-fuels devices.

Techno-economics and sustainability

Solar fuel devices have been built for both PEC and PV/electrolysis devices, demonstrating achievable laboratory-scale conversion efficiencies. These device efficiencies are calculated as solar-to-hydrogen (STH) efficiency, or more generally solar-to-fuel (STF) efficiency, which is defined as the amount of chemical energy produced in the form of the fuel — for example, hydrogen and/or carbon-based fuel(s) — divided by the solar energy input, with no externally applied bias[2]. Advancements in STH efficiency for laboratory-scale electrochemical water splitting devices over the past few decades have been tracked and show steady improvement for both particle-[3] and panel-based[4] systems. Particle-based PEC systems typically achieve lower than 1% STH efficiency, with only a few exceptions, whereas panel-based PEC devices are currently more technologically developed and demonstrate far superior performance. A few notable devices include an integrated PEC/PV device using III–V semiconductor absorbers (one semiconductor–liquid junction (SCLJ) and one buried p–n junction) plus an integrated catalyst for the HER and a decoupled wired catalyst for the oxygen evolution reaction (OER), which achieved 12.4% STH efficiency[5]. Another device, using III–V semiconductor absorbers and integrated catalysts, but including no SCLJs, achieved 18.3% STH efficiency[6]. Fully decoupled PV/electrolysis devices have achieved STH efficiencies greater than 22% as reported recently[7], and some have taken advantage of using various combinations of photoabsorbers and electrolyser devices connected in series to optimize the voltage supply and demand to achieve STH efficiencies up to 30.0%[8–10]. In addition to improving the efficiency of devices, there is a great need to improve device stability, as most reports demonstrate less than 24 hours of device operation[4]. Procedures detailing accurate STH/STF efficiency calculation have been reported[2], but there remains a need to develop broadly accepted standard procedures for long-term stability testing[11].

Tracking the progress of device efficiency for CO_2 reduction is more complicated as the fuel, or mix of fuels, needs to be specified when calculating the efficiency. For example, the best reported solar-to-CO conversion efficiency for solar-driven CO_2 reduction is 6.5%,

[1]SUNCAT Center for Interface Science and Catalysis, Department of Chemical Engineering, Stanford University, Shriram Center, 443 Via Ortega, Stanford, California 94305, USA. [2]SLAC National Accelerator Laboratory, 2575 Sand Hill Road, Menlo Park, California 94025, USA. †Present addresses: Energy Technologies Area, Lawrence Berkeley National Laboratory, 1 Cyclotron Road, Berkeley, California 94720, USA (J.H.M.); Institute for Photon Science and Synchrotron Radiation, Karlsruhe Institute of Technology (KIT), Hermann-von-Helmholtz-Platz 1, 76344 Eggenstein-Leopoldshafen, Germany (L.C.S.). *e-mail: norskov@stanford.edu

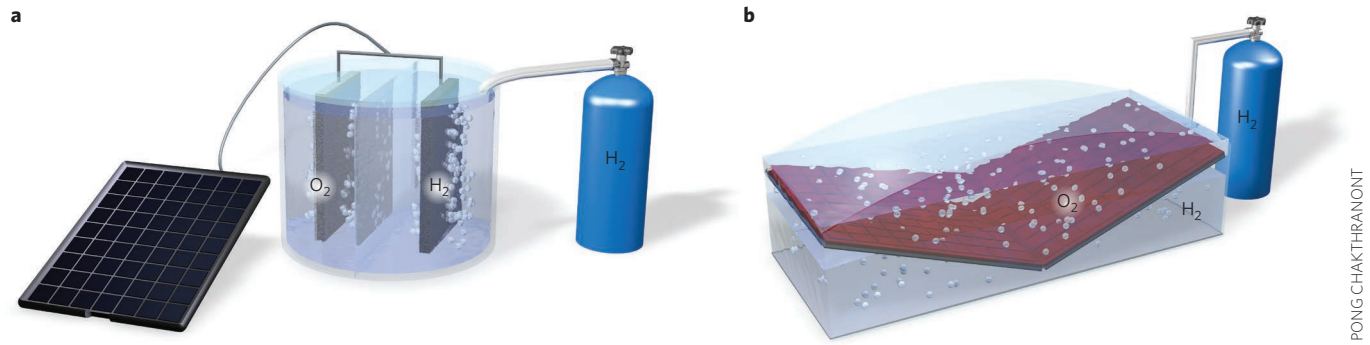

Figure 1 | Diagrams comparing PV/electrolysis and PEC devices for production of solar fuels, showing products for electrochemical water splitting. **a**, PV/electrolysis device. **b**, PEC device.

with hydrogen as a secondary product (7% STH efficiency)[12]. This device consisted of three series-connected perovskite PVs coupled to an IrO_2 anode and a roughened Au cathode, and was operated with high selectivity towards CO for almost 20 hours. A notable device with a reported STF efficiency for CO_2 reduction achieved 4.6% solar-to-formate efficiency using a monolithic tablet-shaped device with IrO_x catalysts at the anode, a ruthenium complex polymer catalyst at the cathode, and a triple junction amorphous silicon germanium photoabsorber[13]. Other studies have focussed on solar-driven CO_2 reduction to CO, formate, methane and methanol, but many do not report or calculate true STF efficiencies[14,15].

Beyond these laboratory-scale examples of devices for the electrochemical production of solar fuels, it is instructive to calculate theoretical efficiency limits, which provide guidance towards future directions. One of the seminal derivations of solar conversion efficiencies, framed in the context of PV devices, was developed by Shockley and Queisser[16], and later expanded on by Ross[17]. Further works[18–21] elaborate on solar conversion efficiencies taking into account losses specific to PEC systems, such as the kinetic overpotentials required to drive electrochemical reactions. These analyses have been continually expanded and updated to consider a range of device performances, from maximum thermodynamically achievable efficiencies to more practical limits considering the current state of materials research. With more complex models being developed, additional factors such as device configuration, number and shape of photoabsorbers, free energy losses (due to blackbody radiation and recombination), catalyst activities, product crossover, solution ohmic resistance and even parasitic photoabsorption in the water layer above a submerged photoabsorber have been incorporated in various published calculations[22–26]. Overall results for these analyses suggest that reasonably achievable PEC water splitting STH efficiencies for single absorber devices are in the range of 10–15% STH efficiency for semiconductors with bandgaps of approximately 1.7–2.2 eV; this is quite a bit lower than the calculated thermodynamic limit of 29–34%[27,28]. Similarly, dual absorber PEC devices should be able to achieve >25% STH efficiency, as illustrated in the contour plot in Fig. 2a, when pairing optimal top and bottom semiconductor absorbers with bandgaps of approximately 1.6–2.0 eV and 0.8–1.4 eV, respectively. Thermodynamically achievable efficiencies for dual absorber PEC devices reach up to 41%[27,28]. Figure 2b shows results from a model similar to Fig. 1b, plotting STH efficiencies for a dual absorber PEC device as a function of overpotentials for the HER and the OER. The black markers identify maximum theoretical efficiencies for devices using combinations of published catalyst activities[29–39]; these calculations highlight the need for developing more active catalysts, especially for the OER. Furthermore, none of these exact combinations have yet been realized, and efficiencies of actual devices are significantly lower than predicted here. It is interesting to note that actual efficiencies of currently reported PEC or PV/electrolysis water splitting devices are much further from predicted theoretical efficiencies compared to PV devices, which are experimentally much closer to achieving their theoretical limit. Additional losses beyond the factors considered in PV modelling include possible voltage supply/demand mismatch between the solar absorbers and the electrochemical reaction of interest, as well as losses at material interfaces.

A complementary analysis for the maximum possible thermodynamic and reasonably achievable STF efficiencies was completed for CO_2 reduction[40]. A combination of PEC and PV/electrolyser designs were considered for single, dual and triple absorber systems that were matched to varying electrochemical load curves for the multitude of possible CO_2RR products (hydrogen, carbon monoxide, formate, methanol, methane, ethanol and ethane). Thermodynamic STF efficiency limits for CO_2RR products were calculated to be approximately 20–25% for single absorber systems, 32–42% for dual absorber systems and 23–33% for triple absorber systems. Dual absorber systems resulted in the highest possible thermodynamic STF efficiencies, as the voltage supply of such a system is better matched to an electrochemical load in the range of 1–2 V, which covers the thermodynamic potential required for most CO_2 reduction products. However, reasonably achievable STF efficiencies considering activities of silver and copper catalysts were predicted to be much lower. Total maximum STF efficiencies of approximately 18% and 14% were calculated for triple and dual absorber systems, respectively, for CO_2 reduction on silver, while total maximum STF efficiencies of approximately 20% and 15% were the corresponding calculated values for CO_2 reduction on copper. These calculations are more representative of the current state of materials research and agree fairly well with recent reports[14,15] of device efficiencies for CO_2 reduction. In these cases, triple absorber systems were predicted to have higher efficiencies due to the additional voltage required to drive CO_2 reduction measured from actual catalysts. These results indicate the potential for improving the efficiency of electrochemical CO_2 reduction devices and highlight the importance of further catalyst development. Additionally, matching of voltage supply to the electrochemical demand will be key to improving efficiencies of solar fuels production devices, which can be difficult for CO_2 reduction due to the range of electrochemical loads possible for different products.

Having established a basis for currently demonstrated and reasonably achievable efficiencies for electrochemical solar fuels production, the next step towards assessing the potential for implementing this technology on a large scale requires additional technical and economic insights. To this effect, the United States Department of Energy (DOE) contracted a detailed evaluation of PEC hydrogen generation based on conceptual systems formulated by the DOE PEC Working Group, including two particle-based systems and two panel-based systems (one with a solar concentrator)

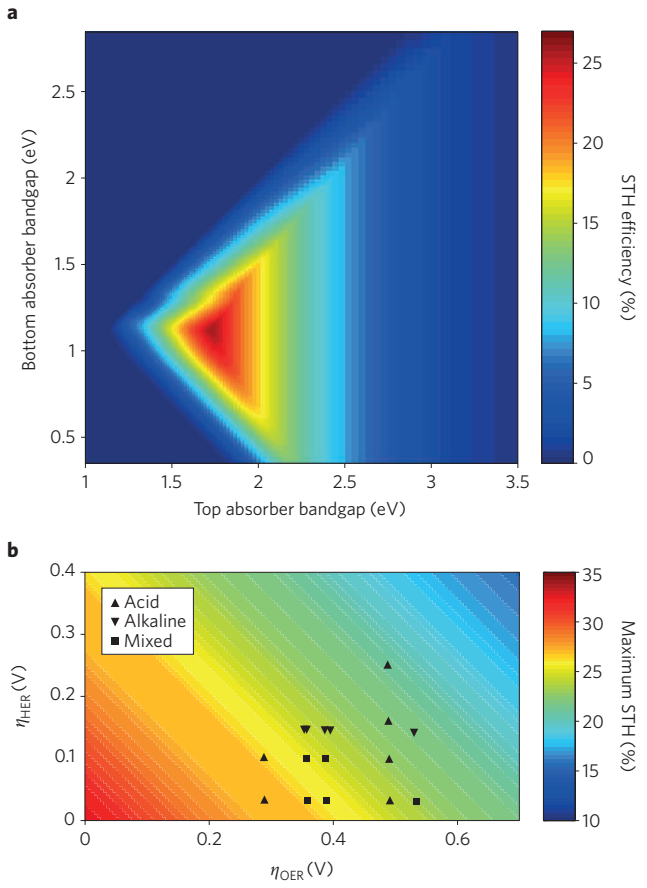

Figure 2 | STH efficiency contour plots as a function of bandgaps and electrocatalytic overpotentials for the top and bottom absorbers of a dual (stacked) absorber PEC water splitting device. a, Calculated STH efficiencies are modelled using some of the most active catalysts for the HER (Pt) and the OER ($NiFeO_x$), and free energy losses equalling approximately 15–30% of the total bandgap of each semiconductor absorber. **b**, Dependence of the maximum achievable STH efficiency as a function of overpotential for the hydrogen evolution reaction (η_{HER}) and the oxygen evolution reaction (η_{OER}), based on published catalyst activities using geometric area normalized current densities, with data points showing potential devices for acid only, alkaline only, or mixed systems[29–39].

for a large-scale PEC hydrogen production plant[41,42]. Particle-based systems were predicted to deliver less expensive hydrogen (US$1.60–3.20 kg^{-1} H_2), but the model's baseline assumptions for operating efficiencies (5–10% STH) were much higher than those of demonstrated particulate-based systems to date. Panel-based systems were predicted be more costly (US$4.00–10.40 kg^{-1} H_2) using baseline assumptions, primarily due to higher estimated reactor material costs, despite better performance (10–15% STH). Furthermore, a sensitivity analysis on all four systems revealed that the STH efficiency had the biggest impact on final hydrogen cost for each system type, although efficiency, stability and material cost are all important factors. Overall, the key message was that PEC water splitting may be able to produce hydrogen economically if appropriate advancements are made towards developing materials that possess sufficient efficiency and stability at reasonable cost to achieve economic targets, for example, STH efficiencies in the 5–25% range and stabilities in the 5–20 year range, depending on the type of reactor and plant design. This highlights the importance of continually improving device performance and cost to bring these technologies towards economical implementation.

Life cycle analyses have also been conducted to assess the net energetics of production, utilization and decommissioning of a hypothetical large-scale PEC water splitting plant[43,44]. Similarly to the technical and economic feasibility analysis, the most important model parameters affecting the net energy metrics were the STH conversion efficiency and the life span of the PEC cells. However, a sensitivity analysis was also conducted considering other parameters relating to the balance of systems (panels, plant area, facility needs), including construction and operation of the liquid and gas handling infrastructure. Such analyses help to determine the potential contribution of technologies towards true sustainability. Further theoretical investigations of the scientific, engineering and economic challenges of electrochemical fuel production are necessary to provide additional insights and more comprehensive understanding such that the community can continue to advance these technologies.

Photon capture

Development of solar fuels devices begins with identifying and developing appropriate materials for photon capture. Recent review articles and books have described in depth the material requirements of solar absorbers for electrochemical fuel production, tracked progress in the development of such materials and identified emerging fields of research[45–47]. As is clear from these studies, there is a wide range of absorber materials that have been investigated, including oxides, oxynitrides, chalcogenides, carbon and carbon nitride-based materials, as well as traditional semiconductors (III–V and, more recently, III–V nitrides). However, there is currently no single material that fulfils all of the requirements for PEC fuel production. The photoabsorber must have an appropriate bandgap and band structure to absorb a large portion of the available solar flux and provide a sufficient driving force for the relevant electrochemical reactions. Additionally, it must have good charge transport properties and long-term stability, while ideally consisting of inexpensive, non-toxic and abundant elements. Owing to the many requirements for PEC fuel production, research efforts have steered towards using multiple photoabsorbers, as addressed in the previous section, in addition to incorporating protection layers and catalysts to the absorber surfaces.

As well as improving the performance of known materials, there is a drive in the solar fuels community to develop new absorber materials, which has led to implementation of experimental screening studies. One such screening study used metal organic deposition to print spots of thin, porous films targeting binary oxides for n-type (Fe-based) and p-type (Bi-based) semiconductors[48]. From this study, $FeVO_4$ and $CuBi_2O_4$ were identified as visible-light-responsive semiconductors. A subsequent study took the screening a step further to investigate ternary oxides based on the Cu–Bi system and identified a Bi–Ag–Cu oxide that has even greater photocurrent than the original $CuBi_2O_4$ (ref. 49). Automated experimental screening studies have greatly increased the rate of discovery of new absorber materials. However, given the enormous phase space of materials to explore, the possibility of missing important materials still remains.

Theoretical efforts towards screening for optical and thermodynamic properties for water splitting photoelectrocatalysis provide a complementary approach to materials discovery. Such efforts have also yielded a number of candidate materials. While traditional semi-local density functional theory (DFT) methods are typically unsuitable for accurate determination of bandgaps, collaborative efforts from the Materials Project[50] and the Computational Materials Repository[51] have shown that thermodynamics from traditional DFT can be combined with higher level methods[52–55] for band structure calculations to evaluate large numbers of photoabsorber candidates on the high-throughput scale[56].

In these computational screening studies, materials are filtered on progressively more selective criteria, which typically begin with bulk phase stability against decomposition. Minimal criteria for single-material photoabsorbers exclude materials with bandgaps that are too high to effectively use sunlight (>3.0 eV) and too small to harvest the energy necessary to split water (<1.23 eV). Tandem photoabsorbers may allow for greater overall effiency[25] and alleviate the lower bound, but add a constraint that combined materials must have sufficiently distinct bandgaps to absorb different portions of the solar spectrum. For both cases, the overall band edge positions must straddle the redox potentials of the HER and OER half-reactions. Ideally, new candidates should also be inexpensive and non-toxic, and provide sufficient photovoltage to overcome the kinetic overpotentials of their respective half-reactions, which combined are at least 0.3 V with the best catalysts.

These strategies are implemented in two landmark initial screening studies[57,58] spanning more than 9,000 nitrides, oxynitrides and perovskite bulk materials. A further screening effort[59] of materials suitable for one- or two-photon water splitting photoabsorption systems evaluates metal oxides, sulfides, nitrides, fluorides and various combinations of their constituent chemistries to screen for an ideal combination of band structures. Many existing compounds known to have water-splitting properties emerged as hits using these strategies, giving confidence to the methodology, and new compounds not yet verified in experiment have also been proposed. At least one material predicted to have optical properties suitable for total water splitting from DFT calculations, $Mn_2V_2O_7$, has been confirmed experimentally[60]. In addition, structure–property relationships, illustrated in an example of how lattices in organometal halide perovskites (OMHPs) influence the band structure[61], may be the most valuable product of high-throughput screening studies, given the inherent inaccuracies in DFT and the highly ideal materials it simulates. However, significant challenges to finding optimal photoabsorber materials remain for both theory and experiment.

One of the most important of these challenges is ensuring the stability of photoabsorber materials under PEC conditions. OMHP materials may be promising, as evidenced by recent reports of total water splitting devices constructed from Earth-abundant materials[62]. However, these and many other new photoabsorber materials are inherently unstable in electrolyte. Furthermore, the structure of materials in devices may be more complex than what is probed in these initial screening studies, which test and synthesize highly ordered, defect-free materials. Developing the theoretical understanding and the experimental methodology to screen materials with truly comprehensive criteria and considering relevant nuances is a significant challenge, but a necessary one to overcome if total PEC devices are to be engineered from first principles.

Catalyst design

Developing effective catalysts to facilitate the bond-making and bond-breaking reactions that occur at the electrode–electrolyte interface is a key criterion for improving the efficiency of future generations of PEC devices. In Fig. 3, we summarize how different state-of-the-art catalysts for the HER[31,32,39,63–68] and OER[36–38,69–71] half-reactions contribute to PEC energy losses in the form of kinetic overpotentials. OER overpotentials are particularly high, even for precious materials such as IrO_2 and RuO_2, and designing catalysts using Earth-abundant materials for either the HER and OER represents an even more difficult challenge[31,32].

In recent years, DFT-based simulations of the electronic structure of catalyst surfaces have yielded both insights into and predictions of advanced materials for HER[72–76], OER[77–80] and CO_2RR[81–84]. This physical framework is used to estimate the free energy changes corresponding to elementary steps involving proton-coupled electron transfer (PCET) on the catalyst surface. Using the computational hydrogen electrode[85], the minimum applied potential required to shift the free energies such that each reaction step is exergonic can then be calculated, and is defined as the limiting potential (U_L) for a given reaction[81,85]. Comparing U_L to the reversible potential for the overall reaction then yields the theoretical overpotential (η_{theor}), which can be used to estimate comparative electrocatalytic performance for materials. Note that η_{theor} is derived exclusively from the thermodynamics of intermediate states in a reaction mechanism[86–89]. Clearly, the next level of understanding will have to involve understanding trends in activation barriers. The notion so far is that they scale with reaction energies.

In the HER, the H* adsorption free energy descriptor provides an explicit estimate of η_{theor}, as the free energy diagram includes only that intermediate. This analysis provides a simple and robust framework for comparing the performance of different electrocatalysts for the HER. In Fig. 4a, we show the results from such an analysis that may be used to screen multi-metallic systems for HER

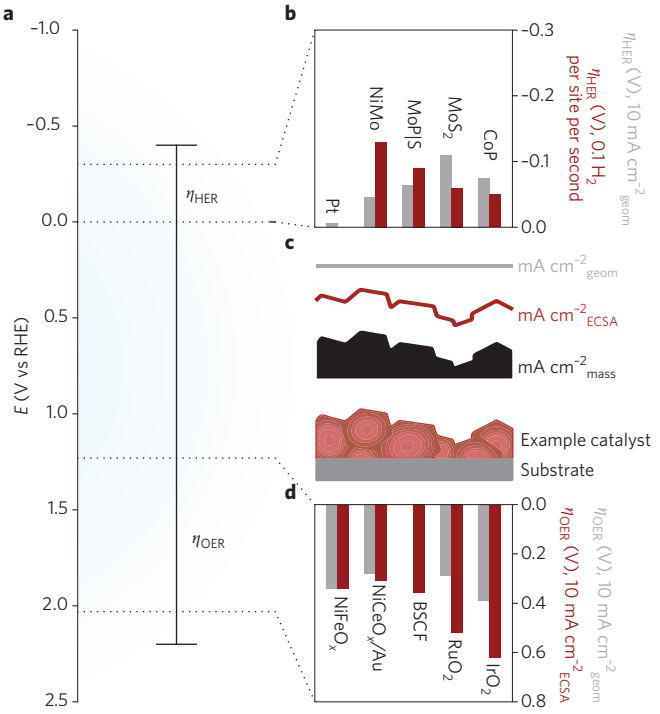

Figure 3 | Losses from experimentally measured electrocatalytic overpotentials for HER and OER. a, Standard band diagram from water splitting relative to the reversible hydrogen electrode (RHE), for reference. **b**, HER overpotential data for MoS_2 (refs 68,92), CoP (refs 39,153), MoS|P (refs 31,64), Pt (ref. 31) and NiMo (refs 65–67,69) are shown as the overpotential required to achieve 10 mA cm^{-2} geometric area (grey) and 0.1 turnover frequency (TOF, red). Note the disparity in overpotentials required for the chosen edge site TOF and geometric current density for MoS_2, which occurs due to MoS_2 having significantly more active edge sites than those on the basal planes. Note also that 0.1 TOF does not reflect performance requirements for PEC, and is included to provide a comparison of intrinsic activity that can be determined for each of the included materials. **c**, Inset diagram of a model catalyst surface illustrating how electrode geometric area, ECSA and mass loading of a catalyst may differ, demonstrating the need for surface area and active site normalized measures of activity to compare intrinsic performance of individual catalysts. **d**, OER overpotential data for IrO_2 (refs 37,69), RuO_2 (refs 37,69), BSCF (ref. 36), $NiCeO_x$/Au (ref. 38) and $NiFeO_x$ (refs 69–71) are shown as the overpotential required to achieve 10 mA cm^{-2} geometric area (grey) and electrochemically active surface area (ECSA) of catalyst (red).

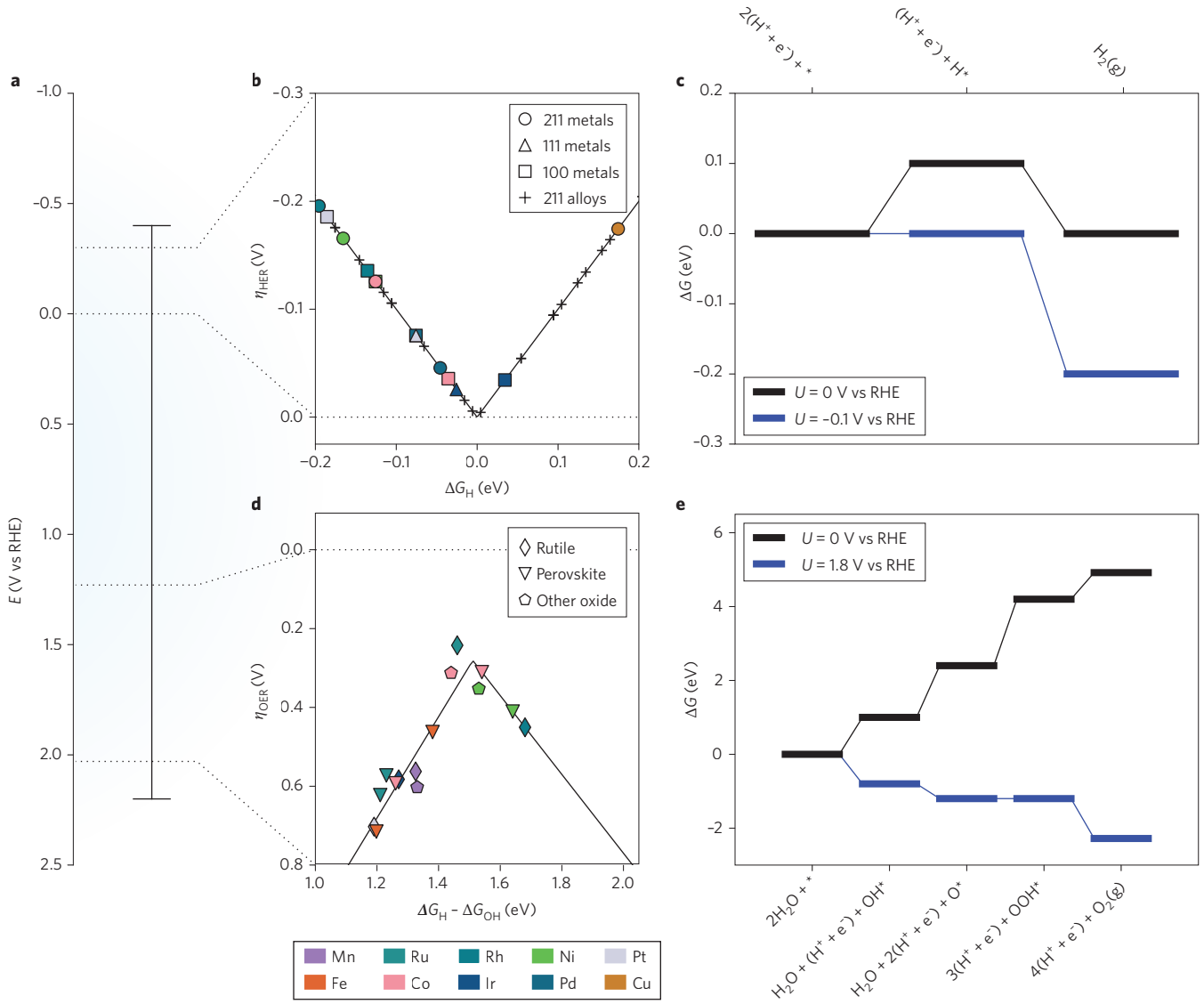

Figure 4 | Standard 'volcano' analysis of η_{theor} for HER and OER using adsorption free energy descriptors from DFT calculations[72,77]. **a**–**e**, Volcano plot overpotentials are shown in relation to standard band diagrams for solar water splitting photoabsorbers (**a**). HER η_{theor} values (**b**) include data corresponding to pure transition metals and metal alloys[90], and OER η_{theor} values (**d**) include rutile, oxide and other common oxide materials[77]. The free energy diagrams (**c**,**e**) are shown proceeding through a single HER intermediate (H*) and three OER intermediates (OH*, O*, OOH*) at applied potentials (*U*) of 0 V vs RHE and 1.8 V vs RHE.

activity[72] using recent data[90]. This descriptor-based approach was also used to successfully model activity in nitrogenase and dehydrogenase enzymes[91], and to identify MoS_2 edge sites as HER active[73], which led to the discovery[92] and development[33,93–98] of a number of new dichalcogenide catalysts for HER. Binary and ternary phosphide materials have more recently been developed for HER[31,99] with similar insights from theory[64]. We also note that, while most materials are limited only by their reactivity towards hydrogen, some oxophilic catalysts may be poisoned by OH* if hydroxyl adsorption is exergonic at negative potentials. If the potential required to favour the reduction of adsorbed OH* is less negative than that required to drive HER, then this potential may be relevant in determining η_{theor}.

The OER mechanism most commonly used to assess catalyst activity in DFT-based studies includes three key intermediates: OH*, O* and OOH*. In principle, a given catalyst might be limited by any of four reaction steps. However, in most materials, OER's η_{theor} is determined by the oxidation of OH* to form O*, or the subsequent attack and oxidation of H_2O on O* to make OOH*. In addition, as shown in Fig. 5a, two key intermediate adsorption free energies ΔG_{OH} and ΔG_{OOH} exhibit a strong linear correlation. A similar bond order of the surface–oxygen bond in OH* and OOH* causes these descriptors to scale with a slope of approximately one, meaning the difference between ΔG_{OH} and ΔG_{OOH} is 3.2 ± 0.2 eV for large classes of catalyst materials[77]. The O* intermediate bridges OH* and OOH* states, meaning that the difference between ΔG_O and ΔG_{OH} effectively describes the overpotential for most OER catalysts. A volcano based on this single descriptor[77] is shown in Fig. 4d and establishes a fairly universal principle by which OER catalyst activity may be described. However, in the best case, if ΔG_O for a given material lies precisely at 1.6 eV above ΔG_{OH} (and therefore 1.6 eV below ΔG_{OOH}), the material should still have an overpotential of at least 0.3 V (1.6–1.23 V). This insight from theory is borne out in experiment, as benchmarking of state-of-the-art

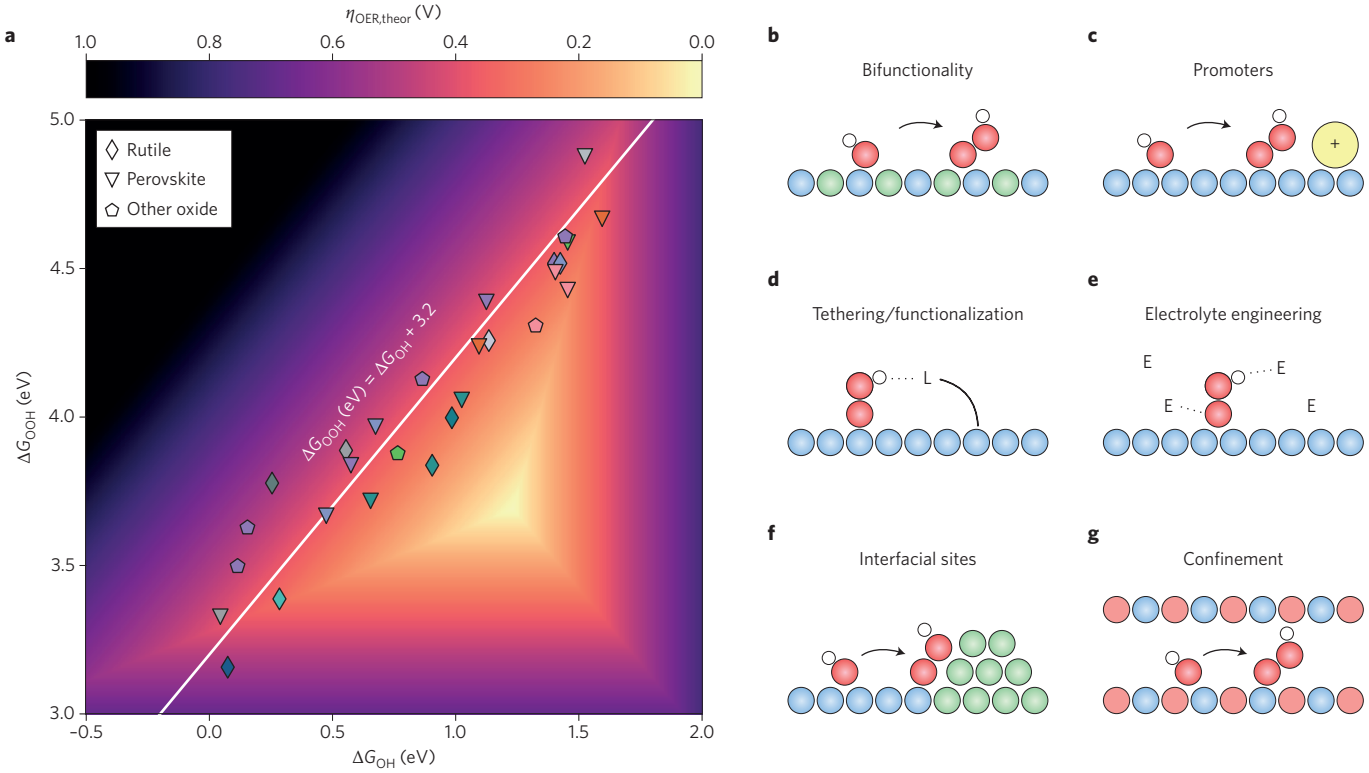

Figure 5 | Catalyst design strategies for tuning adsorption energies towards higher electrocatalytic activity. a, Traditional linear OH*–OOH* scaling relation on a heat map of activity as a function of both variables, showing how the scaling relation deviates from the ideal combination of both. **b**–**g**, Examples of how individual adsorbates in a reaction pathway might be selectively stabilized or destabilized via interactions from their environment. Bifunctionality (**b**) on alloys or binary materials such as sulfides can create a more complex $\Delta G_{OH}/\Delta G_{OOH}$ or $\Delta G_{CO}/\Delta G_{CHO}$ phase space in the CO_2 electroreduction pathway. Promoters, ligands (L) and advanced electrolyte molecules (E) that interact with adsorbates (**c**–**e**) may perturb adsorption energies in a favourable way or enable PCET pathways more selective to CO_2 conversion. Engineering of three-dimensional active sites at interfaces and in confined structures (**f**,**g**) may also enable selective stabilization of adsorbates based on geometry. Differently coloured circles indicate distinct elements.

OER catalysts[36–38,69–71] (Fig. 3d) from the past half-century seems to approach, but barely surpass, this value for the overpotential at which 10 mA cm^{-2} densities are achieved[100].

The CO_2RR is considerably more complex than either the HER or OER, given the wide range of products[101] and multiple PCET steps required to describe mechanisms connecting CO_2 to any product downstream of CO. Furthermore, overpotential limitations in CO_2 catalysis are more severe even than OER at around 1 V to reach a 10 mA cm^{-2} yield of hydrocarbons or alcohols on Cu catalysts[101–103]. However, for Cu and more reactive metal surfaces such as Pt, the further reduction of adsorbed CO to formyl (CHO*) or *COH most severely limits η_{theor} (refs 81,82,104). For less reactive metals such as Au and Ag, initial adsorption and reduction of CO_2 to form adsorbed carboxyl (COOH*) determines η_{theor} (ref. 82).

Fundamental limits on the value of η_{theor} imposed by the scaling relations between free energies of key intermediates and transition states hinder efforts to improve catalysts for the production of solar fuels, particularly with respect to OER and CO_2RR. However, understanding these limitations also has resulted in emerging strategies that target new systems with properties designed to enhance activity[105]. If, for example, if it is possible to fix the OH* adsorption free energy at ~1.23 eV and stabilize the OOH* adsorbate, the portion of the volcano shown in Fig. 5a with OER overpotentials approaching 0 V might be unlocked. Such a selective stabilization has been demonstrated theoretically by confining intermediates in a pore or channel[106] (Fig. 5g), such that a surface opposite to the adsorbate bond stabilizes the OOH* adsorbate via a hydrogen bond, but is not close enough to interact with OH*.

Such multi-functional behaviour might also be achieved using an alloy, binary oxide, or promoter-functionalized surface (Fig. 5b,c) if the adsorbate has the capacity for distinct interactions between the constituents of a multi-component material. For OER and CO_2RR catalysis, the geometries of OOH* and CHO* (or, in fact, the transition states leading to these intermediates) relative to the surface may allow for such a selective interaction between pendant oxygen and neighbouring surface atoms, as their OH* and CO* precursors may have more limited interactions. Selective interactions between different chemical functionalities within surfaces might also be achieved with ligands tethered to a surface (Fig. 5d). Recent progress in CO_2 electroreduction to CO in ionic liquids[107–109] suggests that electrolyte engineering may also tune adsorption or PCET energetics to enhance activity (Fig. 5e). Multi-functional surfaces and interfacial sites (Fig. 5f) may also allow different intermediates to bind to different active sites, as shown previously for CO_2RR intermediates on sulfides[83] and OER intermediates on Ni or Co-doped RuO_2[80]. Interfacial sites at grain boundaries of Cu may also play a role in the activity of oxide-derived materials for CO_2 electroreduction[110–112].

Effectively coupling theory and experiment in the field of electrocatalyst development requires consistent standard metrics of activity that should reflect theoretical trends. Recent efforts to standardize electrochemical catalyst testing have made significant strides by designing and reporting procedures for surface area, activity and short-term stability measurements[69,100]. Measuring an intrinsic activity based on available active sites or true surface area is still a challenge, and the various techniques reported in literature have distinct advantages and disadvantages. Capacitance measurements,

for example, are complicated with oxide or nonmetallic materials for which the intrinsic capacitances are poorly defined and can change with respect to the voltage range tested. Additionally, one can unknowingly measure pseudocapacitive processes and reach inaccurate surface area estimates. Physical methods such as atomic force microscopy can be used but only for very flat, uniform films, and Brunauer–Emmett–Teller gas adsorption, popular in heterogeneous gas-phase catalysis, can be used on powder materials if a sufficient amount can be produced. While not truly intrinsic, activity normalized to total catalyst mass is often an appropriate practical metric for precious-metal-based catalysts, as the scarcity of those materials is a concern. However, advancing our scientific understanding of electrocatalysis requires accurate comparisons of electrocatalytic performance on a per-site basis. Therefore, it is important not only to acknowledge and address the limitations of each surface area measurement technique, but also to work towards improving these techniques.

Given the apparent need for complex materials in PEC co-catalysts, a key scientific challenge also remains for theorists. While models that describe the catalytic activity of metals and speak to the underlying cause of linear scaling relations are well known[113], more general principles that can relate electronic structure to the surface reactivity of promising complex materials[114–116] have been elusive and may require approaches to first-principles simulation beyond generalized gradient approximation-based DFT. Theoretical approaches must be improved to allow for more comprehensive descriptions of electrocatalyst kinetics, including understanding of trends in potential-dependent reaction barriers.

Integration

In its simplest form, a photoelectrode consists of a single active material capable of handling the key processes involved in solar fuel generation: absorption of solar photon energy, charge separation and transport, and catalysis at the surface to use the photogenerated charge carriers efficiently to make and break chemical bonds of interest[117]. In practice, developing a single material to handle all of these functions simultaneously has been challenging. In the aforementioned DFT-based screening studies to identify water splitting photoabsorbers with reasonable band structures, adding the necessary surface chemistry criteria yields essentially no viable candidates that can efficiently absorb a large portion of the solar spectrum and drive both HER and OER at high turnover rates[118]. As such, in recent years there has been an increasing effort to develop multi-component systems that integrate different materials with more specialized functions, for example, combining efficient solar photoabsorbers with high-turnover co-catalysts. This represents an entirely different strategy from aiming to discover a single material that has both the correct band structure and appropriate surface properties for water splitting.

Generally, PEC photoabsorber materials can be classified as conventional PV-grade semiconductors and non-PV-grade semiconductors. PV-grade semiconductors, which are widely used in the PV community due to their superior charge transport properties, include Si, III–V materials (for example, GaAs) and chalcogenides (for example, CIGS, CdTe), among others, while the list of non-PV-grade semiconductors is extremely broad, including metal oxides, transition metal nitrides, carbon-based materials and other emerging semiconductors. Solar fuels devices made with PV-grade and non-PV-grade materials usually use different means to separate the photogenerated charges. Devices with PV-grade semiconductors usually employ a solid-state buried junction[119], which requires additional fabrication steps that can increase cost, but with a major benefit of improved performance, generally leading to higher device efficiencies. Unfortunately, however, PV-grade materials are generally prone to corrosion and exhibit poor stability in aqueous solution. Devices made with non-PV-grade semiconductors generally do not involve the fabrication of a solid-state junction, relying on band-bending at the SCLJ to separate charges. In principle, an SCLJ device is less costly to fabricate and many non-PV-grade materials exhibit greater intrinsic stability than PV-grade devices[120]; however, their performance is extremely sensitive to the physical and chemical properties of the semiconductor–electrolyte interface[121].

Integration of an electrocatalyst for the HER, OER or CO_2RR onto the surface of a photoabsorber often improves the performance of the device, but the role of the catalyst overlayers can be complex. The common functions of a catalyst overlayer on a semiconductor surface can be categorized as follows: (1) to catalyse the bond-making and bond-breaking reactions; (2) to passivate the recombination sites; (3) to tune the band structure energetics; and (4) to protect the surface from corrosion.

A simple model where the semiconductor absorbs light and separates photogenerated charges while the catalyst increases the rates of reactions is usually valid for devices that employ a solid-state buried junction[122]. As the junction is buried in the bulk of the semiconductor, charge separation is independent of the semiconductor–catalyst interface. If the catalyst is sufficiently transparent not to block the light, and assuming that a high-quality interface exists between the catalyst and semiconductor, the performance of a buried junction device can be straightforwardly modelled based on its performance as a PV coupled to the catalytic activity of the overlayer. This concept is apparent in a Si photocathode system. As shown in Fig. 6a, Si photocathodes integrated with various HER catalysts exhibit a monotonic shift in the voltage dependence of the photocurrent as a function of the overpotentials of the HER catalysts; catalyst overlayers with higher intrinsic HER activity lead to higher performance photocathodes[39,123–126]. However, the integration of co-catalysts on an SCLJ device can alter the interfacial energetics and add complexity to the system beyond the simple model where a catalyst role is decoupled from the photoabsorber role[127].

An important role of a catalyst on an SCLJ device, apart from catalysing the electrochemical reactions, is that of surface state passivation[128]. The presence of surface states on the truncated surfaces of a semiconductor can be detrimental to the device performance, as they may act as charge trapping sites, recombination centres and Fermi level pinning states, especially when the surface state energies are found within the bandgap of the semiconductors[129]. Examples of catalyst layers that have been shown to passivate surface states and reduce losses at the interface include CoOOH and Co–Pi, particularly on Fe_2O_3 photoanodes, which have been identified as having a high density of surface states[130–134]. It has been suggested that Co-based catalysts offer a pathway for photogenerated holes to move away from the recombination centres on the Fe_2O_3 surface, thereby improving the photovoltage of the PEC device[135,136]. Similarly, on a $BiVO_4$ photoanode system, a recent report demonstrates that an FeOOH catalyst can reduce losses at the surface of the $BiVO_4$ (ref. 137). The device performance can be leveraged further by stacking a highly active NiOOH catalyst on the FeOOH layer to increases the rate of the OER (Fig. 6b)[138].

A catalyst overlayer that is electrolyte impermeable can modify the band edge energetics of the semiconductors by transforming the SCLJ, where the band bending is governed by the electrolyte redox potential, to a buried junction, where the bands bend irrespective of the electrolyte redox potential[139]. The differences between these two types of catalyst have been demonstrated by using a dual working electrode capable of independently measuring potentials at the semiconductor and at the catalyst. A porous NiOOH OER catalyst is electrolyte permeable, thus the TiO_2/NiOOH is an SCLJ device, which exhibits a higher obtainable voltage. On the contrary, a dense IrO_x forms a buried junction with the TiO_2 surface, resulting in a small fixed open-circuit voltage caused by the low work function

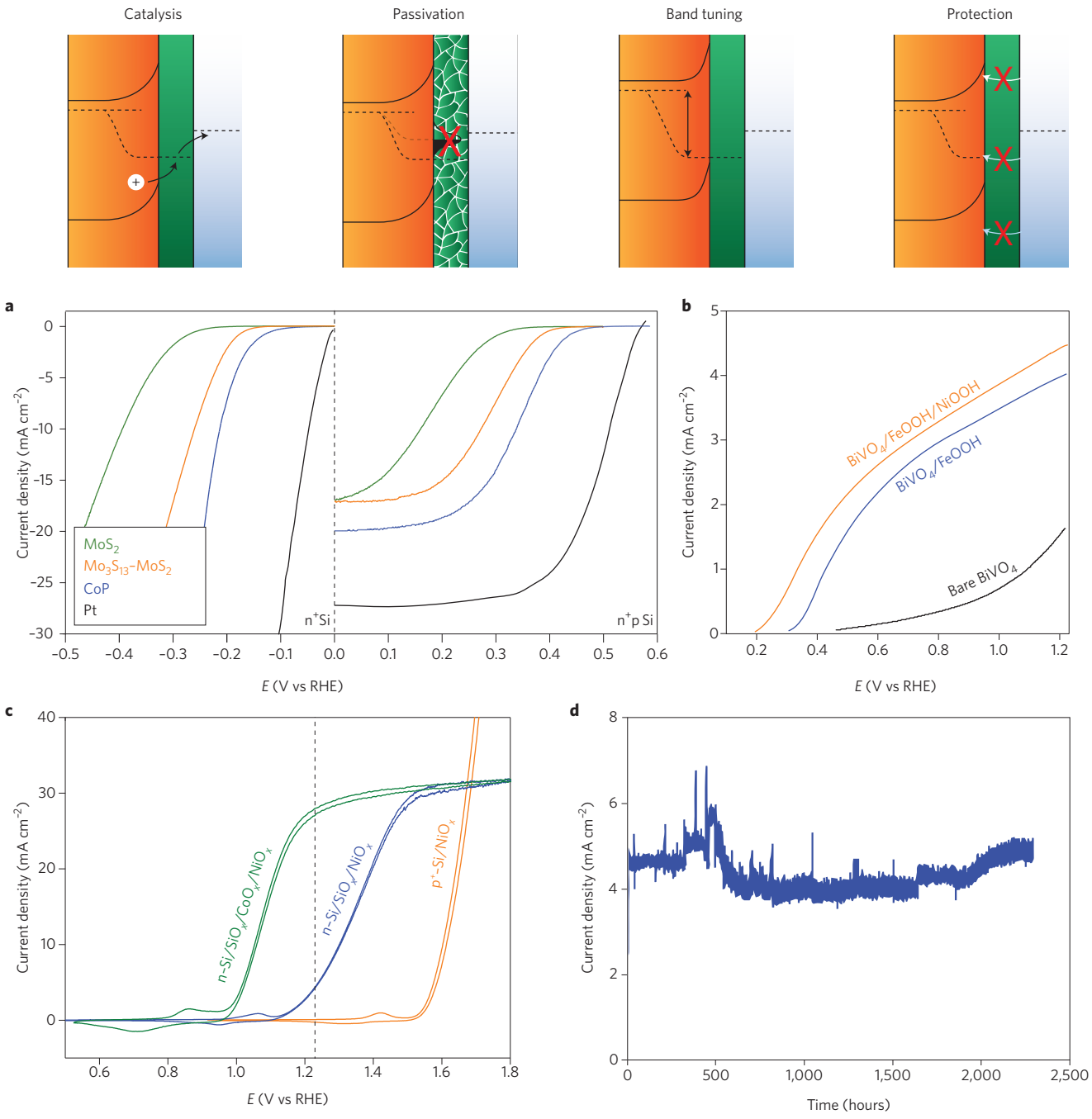

Figure 6 | A catalyst overlayer on a semiconductor surface can improve catalysis, passivate surface states, tune the band energetics and protect the surface from corrosion. a, The photocurrent onsets of p$^+$n Si photocathodes shift linearly with the overpotentials of the HER catalysts. **b**, A highly active $BiVO_4$ photoanode is demonstrated using dual layer FeOOH/NiOOH catalysts that reduce both the interfacial recombination and the OER overpotential. **c**, Overlaying n-Si with 2 nm of CoO_x and sputtered NiO_x yields a heterojunction Si photoanode with as high photovoltage as np$^+$ buried homojunction. **d**, A np$^+$Si/TiO_2/$NiCrO_x$ photoanode is stable after more than 2,200 hours in 1 M KOH under 1 sun intensity. Adapted from ref. 39, Wiley (**a**); ref. 138, AAAS (**b**); ref. 140, RSC (**c**); ref. 149, RSC (**d**).

of IrO_x[139]. As the photovoltage of the buried semiconductor–catalyst junction depends on the work function difference at the semiconductor–catalyst interface, an appropriate catalyst can improve the photovoltage of the photoelectrode, irrespective of the semiconductor band edge locations with respect to the electrolyte redox potential. For example, solid-state buried junctions can be constructed by overlaying NiO_x and CoO_x on an n-type Si photoanode, increasing the photovoltage to as high as that of a conventional n$^+$p junction, as shown in Fig. 6c[140]. Overlaying dipole materials[141] or dipole species[142,143] on a semiconductor can also be employed to shift the band edge positions of a semiconductor up or down on the energy scale, and potentially allow semiconductors with unfavourable band edge positions to be used in a PEC device.

Finally, a catalyst overlayer can improve the stability of the photoabsorber by serving as a corrosion protection layer[144]. Almost all known PEC materials are thermodynamically unstable under operating conditions[145], and one approach to overcome this limitation is to encapsulate the photoabsorber by a physical barrier that

effectively blocks the surface from the harsh reaction conditions. This protection layer must be highly stable but also sufficiently conductive and transparent to maintain high light harvesting efficiency[146]. Several protection schemes with intermediate stability of 24 hours to 30 days have been demonstrated using HER[123,124] or OER[147,148] catalyst layers, with one particular demonstration of stability lasting more than 3 months for a Si photocathode protected by an atomic layer deposited amorphous TiO_2 together with a sputtered $NiCrO_x$ catalyst, shown in Fig. 6d[149]. Building from the recent progress in protection scheme development, more work is needed to understand the mechanisms of failure to improve stability even further, as well as to develop fabrication methods to produce large-scale pinhole-free protection layers that will enable the industrial scale processing of PEC technology.

Given the challenges enumerated above and promise of integrating multiple components into a functional PEC device, improving theoretical methods for the treatment of interfaces between materials would be particularly beneficial. Preliminary efforts towards characterizing the catalyst–semiconductor junction in PEC systems have illustrated that the interfacial effects on both the photovoltage and electrocatalyst active sites may significantly affect PEC activity[150,151]. Therefore, prospects for engineering an effective PEC device would benefit tremendously from a greater understanding of the interface between the paired photoabsorber and co-catalyst by their respective chemistries and nanostructures.

In addition to material development and integration, chemical engineering challenges associated with product separation, device design, pressurized gas handling and ion transport must be addressed to enable deployable and scalable PEC devices. One important requirement for a safe and robust operation of PEC devices is the separation of gas products from the anode and the cathode compartment; hence, a membrane is required to prevent product crossover. To minimize a transport loss and pH gradient across a membrane, the membrane height must be limited, and highly acidic or highly basic electrolyte must be used[22,152]. The limitation in membrane height increases the complexity of cell design and gas product handling, while the extreme pH requirement inhibits the direct use of untreated seawater as a feedstock, leading to an extra cost and a safety concern. While these challenges may ultimately be solved via innovative engineering, they may also impose design criteria for PEC materials, and should be considered accordingly.

Conclusion

Solar fuels research is growing rapidly. While there have already been important advances, the largest scientific and technical milestones are still ahead of us. We conclude by listing some of the scientific challenges that we see as the most important for the coming years.

The biggest challenge for photoabsorber materials is still materials discovery. We are in need of new materials with suitable bandgaps and band edges. Experimental and computational screening of new materials has begun, but there are still many to be simulated and tested. Understanding trends may also enable more effective design of advanced photoabsorbers. Some insights into structure–property relationships have been derived from the large quantity of available band structure data, but there are likely to be a number of trends that might yet be discovered and leveraged into more effective searches. Stability, particularly in the aqueous environment at the electrode interface, will also be a key concern.

For electrocatalysts, there has been remarkable progress in developing new, non-precious metal catalysts for hydrogen evolution recently. There is still significant room for improvement. A larger challenge is to improve the performance of catalysts for the OER. Even the best OER catalysts have overpotentials of 0.3 V or higher, suggesting that OER catalysis faces a fundamental obstacle to reducing overpotential losses that is very difficult to break through. Theory has shown that this overpotential 'wall' may be explained by scaling relationships between the stability of important intermediates for large classes of catalysts. New catalyst design strategies are needed such that the stability of different intermediates and transition states can be varied independently. This is likely to require precise engineering of individual active sites and thus new approaches to designing and synthesizing nanostructured materials.

Creating solar fuels using CO_2 reduction is even more demanding. While reasonably efficient catalysts exist to produce CO from CO_2 (ref. 107), there are no known catalysts producing hydrocarbons or alcohols with high rates and low overpotentials. The current state of the art for hydrocarbon synthesis is still Cu, which requires nearly 1 V of overpotential to produce 10 mA cm^{-2} of products further reduced than CO. As in the OER, scaling relations between CO and further reduced adsorbates explain the difficulty of finding good catalysts, but the understanding of CO_2 reduction electrocatalysis is still in its infancy. In general, an improved molecular-level understanding of chemical processes at the charged solid–liquid interface, and advanced descriptors (experimental and theoretical) of catalytic activity and selectivity will be necessary to screen for new catalysts.

For integrated systems, we need to be able to engineer interfaces between photoabsorber materials and catalysts such that the two materials work together with the lowest losses. Furthermore, we must understand failure mechanisms and respond with scalable protection schemes to make devices more robust.

We are far from having solutions to the production of solar fuels and chemicals, and we cannot rely solely on trial-and-error strategies to solve the challenges ahead. However, by improving fundamental understanding of materials properties relevant to each aspect of the photoelectrocatalytic device that connects the incident photon to the desorbing fuel molecule, we may accelerate the process of making artificial photosynthesis a reality.

Received 4 May 2016; accepted 12 September 2016; published online 20 December 2016

References

1. Appel, A. M. *et al.* Frontiers, opportunities, and challenges in biochemical and chemical catalysis of CO_2 fixation. *Chem. Rev.* **113,** 6621–6658 (2013).
2. Chen, Z. *et al.* Accelerating materials development for photoelectrochemical hydrogen production: standards for methods, definitions, and reporting protocols. *J. Mater. Res.* **25,** 3–16 (2010).
3. Fabian, D. M. *et al.* Particle suspension reactors and materials for solar-driven water splitting. *Energy Environ. Sci.* **8,** 2825–2850 (2015).
4. Ager, J. W., Shaner, M. R., Walczak, K. A., Sharp, I. D. & Ardo, S. Experimental demonstrations of spontaneous, solar-driven photoelectrochemical water splitting. *Energy Environ. Sci.* **8,** 2811–2824 (2015).
5. Khaselev, O. & Turner, J. A monolithic photovoltaic-photoelectrochemical device for hydrogen production via water splitting. *Science* **280,** 425–427 (1998).
6. Licht, S. *et al.* Efficient solar water splitting, exemplified by RuO_2-catalyzed AlGaAs/Si photoelectrolysis. *J. Phys. Chem. B* **104,** 8920–8924 (2000).
7. Bonke, S. A., Wiechen, M., MacFarlane, D. R. & Spiccia, L. Renewable fuels from concentrated solar power: towards practical artificial photosynthesis. *Energy Environ. Sci.* **8,** 2791–2796 (2015).
8. Fujii, K. *et al.* Characteristics of hydrogen generation from water splitting by polymer electrolyte electrochemical cell directly connected with concentrated photovoltaic cell. *Int. J. Hydrogen Energy* **38,** 14424–14432 (2013).
9. Akihiro, N. *et al.* A 24.4% solar to hydrogen energy conversion efficiency by combining concentrator photovoltaic modules and electrochemical cells. *Appl. Phys. Express* **8,** 107101 (2015).
10. Jia, J. *et al.* Solar water splitting by photovoltaic-electrolysis with a solar-to-hydrogen efficiency over 30%. *Nat. Commun.* **7,** 13237 (2016).
11. Chen, Z., Dinh, H. N. & Miller, E. *Photoelectrochemical Water Splitting* (Springer, 2013).
12. Schreier, M. *et al.* Efficient photosynthesis of carbon monoxide from CO_2 using perovskite photovoltaics. *Nat. Commun.* **6,** 7326 (2015).
13. Arai, T., Sato, S. & Morikawa, T. A monolithic device for CO_2 photoreduction to generate liquid organic substances in a single-compartment reactor. *Energy Environ. Sci.* **8,** 1998–2002 (2015).

14. Schreier, M. *et al.* Covalent immobilization of a molecular catalyst on Cu_2O photocathodes for CO_2 reduction. *J. Am. Chem. Soc.* **138,** 1938–1946 (2016).
15. Benedetti, J. E., Bernardo, D. R., Morais, A., Bettini, J. & Nogueira, A. F. Synthesis and characterization of a quaternary nanocomposite based on TiO_2/CdS/rGO/Pt and its application in the photoreduction of CO_2 to methane under visible light. *RSC Adv.* **5,** 33914–33922 (2015).
16. Shockley, W. & Queisser, H. J. Detailed balance limit of efficiency of p–n junction solar cells. *J. Appl. Phys.* **32,** 510–519 (1961).
17. Ross, R. T. Some thermodynamics of photochemical systems. *J. Chem. Phys.* **46,** 4590–4593 (1967).
18. Weber, M. F. & Dignam, M. J. Efficiency of splitting water with semiconducting photoelectrodes. *J. Electrochem. Soc.* **131,** 1258–1265 (1984).
19. Weber, M. & Dignam, M. Splitting water with semiconducting photoelectrodes—efficiency considerations. *Int. J. Hydrogen Energy* **11,** 225–232 (1986).
20. Rocheleau, R. E. & Miller, E. L. Photoelectrochemical production of hydrogen: engineering loss analysis. *Int. J. Hydrogen Energy* **22,** 771–782 (1997).
21. Bolton, J. R., Strickler, S. J. & Connolly, J. S. Limiting and realizable efficiencies of solar photolysis of water. *Nature* **316,** 495–500 (1985).
22. Haussener, S. *et al.* Modeling, simulation, and design criteria for photoelectrochemical water-splitting systems. *Energy Environ. Sci.* **5,** 9922–9935 (2012).
23. Haussener, S., Hu, S., Xiang, C., Weber, A. Z. & Lewis, N. S. Simulations of the irradiation and temperature dependence of the efficiency of tandem photoelectrochemical water-splitting systems. *Energy Environ. Sci.* **6,** 3605–3618 (2013).
24. Hu, S., Xiang, C., Haussener, S., Berger, A. D. & Lewis, N. S. An analysis of the optimal band gaps of light absorbers in integrated tandem photoelectrochemical water-splitting systems. *Energy Environ. Sci.* **6,** 2984–2993 (2013).
25. Seitz, L. C. *et al.* Modeling Practical performance limits of photoelectrochemical water splitting based on the current state of materials research. *ChemSusChem* **7,** 1372–1385 (2014).
26. Döscher, H. *et al.* Sunlight absorption in water-efficiency and design implications for photoelectrochemical devices. *Energy Environ. Sci.* **7,** 2951–2956 (2014).
27. Ross, R. T. & Hsiao, T.-L. Limits on the yield of photochemical solar energy conversion. *J. Appl. Phys.* **48,** 4783–4785 (1977).
28. Hanna, M. C. & Nozik, A. J. Solar conversion efficiency of photovoltaic and photoelectrolysis cells with carrier multiplication absorbers. *J. Appl. Phys.* **100,** 074510 (2006).
29. Sheng, W., Gasteiger, H. A. & Shao-Horn, Y. Hydrogen oxidation and evolution reaction kinetics on platinum: acid vs alkaline electrolytes. *J. Electrochem. Soc.* **157,** B1529–B1536 (2010).
30. Schuldiner, S. Hydrogen overvoltage on bright platinum. *J. Electrochem. Soc.* **99,** 488–494 (1952).
31. Kibsgaard, J. & Jaramillo, T. F. Molybdenum phosphosulfide: an active, acid-stable, Earth-abundant catalyst for the hydrogen evolution reaction. *Angew. Chem. Int. Ed.* **53,** 14433–14437 (2014).
32. Benck, J. D., Hellstern, T. R., Kibsgaard, J., Chakthranont, P. & Jaramillo, T. F. Catalyzing the hydrogen evolution reaction (HER) with molybdenum sulfide nanomaterials. *ACS Catal.* **4,** 3957–3971 (2014).
33. Kibsgaard, J., Chen, Z., Reinecke, B. N. & Jaramillo, T. F. Engineering the surface structure of MoS_2 to preferentially expose active edge sites for electrocatalysis. *Nat. Mater.* **11,** 963–969 (2012).
34. Lee, Y., Suntivich, J., May, K. J., Perry, E. E. & Shao-Horn, Y. Synthesis and activities of rutile IrO_2 and RuO_2 nanoparticles for oxygen evolution in acid and alkaline solutions. *J. Phys. Chem. Lett.* **3,** 399–404 (2012).
35. Trotochaud, L., Ranney, J. K., Williams, K. N. & Boettcher, S. W. Solution-cast metal oxide thin film electrocatalysts for oxygen evolution. *J. Am. Chem. Soc.* **134,** 17253–17261 (2012).
36. Suntivich, J., May, K. J., Gasteiger, H. A., Goodenough, J. B. & Shao-Horn, Y. A perovskite oxide optimized for oxygen evolution catalysis from molecular orbital principles. *Science* **334,** 1383–1385 (2011).
37. Stoerzinger, K. A., Qiao, L., Biegalski, M. D. & Shao-Horn, Y. Orientation-dependent oxygen evolution activities of rutile IrO_2 and RuO_2. *J. Phys. Chem. Lett.* **5,** 1636–1641 (2014).
38. Ng, J. W. D. *et al.* Gold-supported cerium-doped NiO_x catalysts for water oxidation. *Nat. Energy* **1,** 16053 (2016).
39. Hellstern, T. R., Benck, J. D., Kibsgaard, J., Hahn, C. & Jaramillo, T. F. Engineering cobalt phosphide (CoP) thin film catalysts for enhanced hydrogen evolution activity on silicon photocathodes. *Adv. Energy Mater.* **6,** 1501758 (2016).
40. Singh, M. R., Clark, E. L. & Bell, A. T. Thermodynamic and achievable efficiencies for solar-driven electrochemical reduction of carbon dioxide to transportation fuels. *Proc. Natl Acad. Sci. USA* **112,** E6111–E6118 (2015).
41. James, B. D., Baum, G. N., Perez, J. & Baum, K. N. *Technoeconomic Analysis of Photoelectrochemical (PEC) Hydrogen Production* Final Report (US Department of Energy, 2009).
42. Pinaud, B. A. *et al.* Technical and economic feasibility of centralized facilities for solar hydrogen production via photocatalysis and photoelectrochemistry. *Energy Environ. Sci.* **6,** 1983–2002 (2013).
43. Sathre, R. *et al.* Life-cycle net energy assessment of large-scale hydrogen production via photoelectrochemical water splitting. *Energy Environ. Sci.* **7,** 3264–3278 (2014).
44. Sathre, R. *et al.* Opportunities to improve the net energy performance of photoelectrochemical water-splitting technology. *Energy Environ. Sci.* **9,** 803–819 (2016).
45. Sivula, K. & van de Krol, R. Semiconducting materials for photoelectrochemical energy conversion. *Nat. Rev. Mater.* **1,** 15010 (2016).
46. Sugiyama, M., Nakamura, S. & Fujii, K. (eds) *Solar to Chemical Energy Conversion: Theory and Application* (Lecture Notes in Energy Vol. 32, Springer, 2016).
47. Hisatomi, T., Kubota, J. & Domen, K. Recent advances in semiconductors for photocatalytic and photoelectrochemical water splitting. *Chem. Soc. Rev.* **43,** 7520–7535 (2014).
48. Arai, T., Konishi, Y., Iwasaki, Y., Sugihara, H. & Sayama, K. High-throughput screening using porous photoelectrode for the development of visible-light-responsive semiconductors. *J. Comb. Chem.* **9,** 574–581 (2007).
49. Berglund, S. P., Lee, H. C., Nunez, P. D., Bard, A. J. & Mullins, C. B. Screening of transition and post-transition metals to incorporate into copper oxide and copper bismuth oxide for photoelectrochemical hydrogen evolution. *Phys. Chem. Chem. Phys.* **15,** 4554–4565 (2013).
50. Jain, A. *et al.* Commentary: the Materials Project: a materials genome approach to accelerating materials innovation. *APL Mater.* **1,** 011002 (2013).
51. Landis, D. D. *et al.* The Computational Materials Repository. *Comput. Sci. Eng.* **14,** 51–57 (2012).
52. Gritsenko, O., van Leeuwen, R., van Lenthe, E. & Baerends, E. J. Self-consistent approximation to the Kohn–Sham exchange potential. *Phys. Rev. A* **51,** 1944–1954 (1995).
53. Heyd, J., Scuseria, G. E. & Ernzerhof, M. Hybrid functionals based on a screened Coulomb potential. *J. Chem. Phys.* **118,** 8207–8215 (2003).
54. Chan, M. K. Y. & Ceder, G. Efficient band gap prediction for solids. *Phys. Rev. Lett.* **105,** 196403 (2010).
55. Kuisma, M., Ojanen, J., Enkovaara, J. & Rantala, T. T. Kohn–Sham potential with discontinuity for band gap materials. *Phys. Rev. B* **82,** 115106 (2010).
56. Castelli, I. E. *et al.* New light-harvesting materials using accurate and efficient bandgap calculations. *Adv. Energy Mater.* **5,** 1400915 (2015).
57. Castelli, I. E. *et al.* Computational screening of perovskite metal oxides for optimal solar light capture. *Energy Environ. Sci.* **5,** 5814–5819 (2012).
58. Wu, Y., Lazic, P., Hautier, G., Persson, K. & Ceder, G. First principles high throughput screening of oxynitrides for water-splitting photocatalysts. *Energy Environ. Sci.* **6,** 157–168 (2013).
59. Castelli, I. E. *et al.* New cubic perovskites for one- and two-photon water splitting using the computational materials repository. *Energy Environ. Sci.* **5,** 9034–9043 (2012).
60. Yan, Q. *et al.* $Mn_2V_2O_7$: an Earth abundant light absorber for solar water splitting. *Adv. Energy Mater.* **5,** 1401840 (2015).
61. Castelli, I. E., García-Lastra, J. M., Thygesen, K. S. & Jacobsen, K. W. Bandgap calculations and trends of organometal halide perovskites. *APL Mater.* **2,** 081514 (2014).
62. Luo, J. *et al.* Water photolysis at 12.3% efficiency via perovskite photovoltaics and Earth-abundant catalysts. *Science* **345,** 1593–1596 (2014).
63. McCrory, C. C. L. *et al.* Benchmarking hydrogen evolving reaction and oxygen evolving reaction electrocatalysts for solar water splitting devices. *J. Am. Chem. Soc.* **137,** 4347–4357 (2015).
64. Kibsgaard, J. *et al.* Designing an improved transition metal phosphide catalyst for hydrogen evolution using experimental and theoretical trends. *Energy Environ. Sci.* **8,** 3022–3029 (2015).
65. Navarro-Flores, E., Chong, Z. & Omanovic, S. Characterization of Ni, NiMo, NiW and NiFe electroactive coatings as electrocatalysts for hydrogen evolution in an acidic medium. *J. Mol. Catal. A Chem.* **226,** 179–197 (2005).
66. Krstajic, N. *et al.* Electrodeposition of Ni–Mo alloy coatings and their characterization as cathodes for hydrogen evolution in sodium hydroxide solution. *Int. J. Hydrogen Energy* **33,** 3676–3687 (2008).
67. Fan, C. Study of electrodeposited nickel-molybdenum, nickel-tungsten, cobalt-molybdenum, and cobalt-tungsten as hydrogen electrodes in alkaline water electrolysis. *J. Electrochem. Soc.* **141,** 382–387 (1994).
68. Li, D. J. *et al.* Molybdenum sulfide/N-doped CNT forest hybrid catalysts for high-performance hydrogen evolution reaction. *Nano Lett.* **14,** 1228–1233 (2014).
69. McCrory, C. C. L. *et al.* Benchmarking HER and OER electrocatalysts for solar water splitting devices. *J. Am. Chem. Soc.* **137,** 4347–4357 (2015).

70. Trotochaud, L., Young, S. L., Ranney, J. K. & Boettcher, S. W. Nickel-iron oxyhydroxide oxygen-evolution electrocatalysts: the role of intentional and incidental iron incorporation. *J. Am. Chem. Soc.* **136,** 6744–6753 (2014).
71. Louie, M. W. & Bell, A. T. An investigation of thin-film Ni–Fe oxide catalysts for the electrochemical evolution of oxygen. *J. Am. Chem. Soc.* **135,** 12329–12337 (2013).
72. Greeley, J., Jaramillo, T. F., Bonde, J., Chorkendorff, I. B. & Nørskov, J. K. Computational high-throughput screening of electrocatalytic materials for hydrogen evolution. *Nat. Mater.* **5,** 909–913 (2006).
73. Hinnemann, B. *et al.* Biomimetic hydrogen evolution: MoS_2 nanoparticles as catalyst for hydrogen evolution. *J. Am. Chem. Soc.* **127,** 5308–5309 (2005).
74. Bonde, J., Moses, P. G., Jaramillo, T. F., Nørskov, J. K. & Chorkendorff, I. Hydrogen evolution on nano-particulate transition metal sulfides. *Faraday Discuss.* **140,** 219–231 (2009).
75. Canaguier, S. *et al.* Cyclopentadienyl ruthenium-nickel catalysts for biomimetic hydrogen evolution: electrocatalytic properties and mechanistic DFT studies. *Chemistry* **15,** 9350–9364 (2009).
76. Zheng, Y. *et al.* Hydrogen evolution by a metal-free electrocatalyst. *Nat. Commun.* **5,** 3783 (2014).
77. Man, I. C. *et al.* Universality in oxygen evolution electrocatalysis on oxide surfaces. *ChemCatChem* **3,** 1159–1165 (2011).
78. Zhang, J., Zhao, Z., Xia, Z. & Dai, L. A metal-free bifunctional electrocatalyst for oxygen reduction and oxygen evolution reactions. *Nat. Nanotech.* **10,** 444–452 (2015).
79. Viswanathan, V., Pickrahn, K. L., Luntz, A. C., Bent, S. F. & Nørskov, J. K. Nanoscale limitations in metal oxide electrocatalysts for oxygen evolution. *Nano Lett.* **14,** 5853–5857 (2014).
80. Halck, N. B., Petrykin, V., Krtil, P. & Rossmeisl, J. Beyond the volcano limitations in electrocatalysis–oxygen evolution reaction. *Phys. Chem. Chem. Phys.* **16,** 13682–13688 (2014).
81. Peterson, A. A., Abild-Pedersen, F., Studt, F., Rossmeisl, J. & Nørskov, J. K. How copper catalyzes the electroreduction of carbon dioxide into hydrocarbon fuels. *Energy Environ. Sci.* **3,** 1311–1315 (2010).
82. Peterson, A. A. & Nørskov, J. K. Activity descriptors for CO_2 electroreduction to methane on transition-metal catalysts. *J. Phys. Chem. Lett.* **3,** 251–258 (2012).
83. Chan, K., Tsai, C., Hansen, H. A. & Nørskov, J. K. Molybdenum sulfides and selenides as possible electrocatalysts for CO_2 reduction. *ChemCatChem* **6,** 1899–1905 (2014).
84. Hansen, H. A., Shi, C., Lausche, A. C., Peterson, A. A. & Nørskov, J. K. Bifunctional alloys for the electroreduction of CO_2 and CO. *Phys. Chem. Chem. Phys.* **18,** 9194–9201 (2016).
85. Nørskov, J. K. *et al.* Origin of the overpotential for oxygen reduction at a fuel-cell cathode. *J. Phys. Chem. B* **108,** 17886–17892 (2004).
86. Skulason, E. *et al.* Density functional theory calculations for the hydrogen evolution reaction in an electrochemical double layer on the Pt(111) electrode. *Phys. Chem. Chem. Phys.* **9,** 3241–3250 (2007).
87. Rossmeisl, J., Skúlason, E., Björketun, M. E., Tripkovic, V. & Nørskov, J. K. Modeling the electrified solid–liquid interface. *Chem. Phys. Lett.* **466,** 68–71 (2008).
88. Shi, C., O'Grady, C. P., Peterson, A. A., Hansen, H. A. & Nørskov, J. K. Modeling CO_2 reduction on Pt(111). *Phys. Chem. Chem. Phys.* **15,** 7114–7122 (2013).
89. Chan, K. & Nørskov, J. K. Electrochemical barriers made simple. *J. Phys. Chem. Lett.* **6,** 2663–2668 (2015).
90. Tsai, C. *et al.* Direct water decomposition on transition metal surfaces: structural dependence and catalytic screening. *Catal. Lett.* **146,** 718–724 (2016).
91. Hinnemann, B. & Nørskov, J. K. Chemical activity of the nitrogenase FeMo cofactor with a central nitrogen ligand: density functional study. *J. Am. Chem. Soc.* **126,** 3920–3927 (2004).
92. Jaramillo, T. F. *et al.* Identification of active edge sites for electrochemical H_2 evolution from MoS_2 nanocatalysts. *Science* **317,** 100–102 (2007).
93. Chen, Z. *et al.* Core–shell MoO_3–MoS_2 nanowires for hydrogen evolution: a functional design for electrocatalytic materials. *Nano Lett.* **11,** 4168–4175 (2011).
94. Benck, J. D., Chen, Z., Kuritzky, L. Y., Forman, A. J. & Jaramillo, T. F. Amorphous molybdenum sulfide catalysts for electrochemical hydrogen production: insights into the origin of their catalytic activity. *ACS Catal.* **2,** 1916–1923 (2012).
95. Jaramillo, T. F. *et al.* Hydrogen evolution on supported incomplete cubane-type $[Mo_3S_4]^{4+}$ electrocatalysts. *J. Phys. Chem. C* **112,** 17492–17498 (2008).
96. Li, Y. *et al.* MoS_2 nanoparticles grown on graphene: an advanced catalyst for the hydrogen evolution reaction. *J. Am. Chem. Soc.* **133,** 7296–7299 (2011).
97. Kong, D. *et al.* Synthesis of MoS_2 and $MoSe_2$ films with vertically aligned layers. *Nano Lett.* **13,** 1341–1347 (2013).
98. Xiang, Q., Yu, J. & Jaroniec, M. Synergetic effect of MoS_2 and graphene as cocatalysts for enhanced photocatalytic H_2 production activity of TiO_2 nanoparticles. *J. Am. Chem. Soc.* **134,** 6575–6578 (2012).
99. Xiao, P. *et al.* Molybdenum phosphide as an efficient electrocatalyst for the hydrogen evolution reaction. *Energy Environ. Sci.* **7,** 2624–2629 (2014).
100. McCrory, C. C. L., Jung, S., Peters, J. C. & Jaramillo, T. F. Benchmarking heterogeneous electrocatalysts for the oxygen evolution reaction. *J. Am. Chem. Soc.* **135,** 16977–16987 (2013).
101. Kuhl, K. P., Cave, E. R., Abram, D. N. & Jaramillo, T. F. New insights into the electrochemical reduction of carbon dioxide on metallic copper surfaces. *Energy Environ. Sci.* **5,** 7050–7059 (2012).
102. Hori, Y. in *Modern Aspects of Electrochemistry* (eds Vayenas, C. G., White, R. E. & Gamboa-Aldeco, M. E.) 89–189 (Springer, 2008).
103. Kuhl, K. P. *et al.* Electrocatalytic conversion of carbon dioxide to methane and methanol on transition metal surfaces. *J. Am. Chem. Soc.* **136,** 14107–14113 (2014).
104. Nie, X., Esopi, M. R., Janik, M. J. & Asthagiri, A. Selectivity of CO_2 reduction on copper electrodes: the role of the kinetics of elementary steps. *Angew. Chem. Int. Ed.* **52,** 2459–2462 (2013).
105. Vojvodic, A. & Nørskov, J. K. New design paradigm for heterogeneous catalysts. *Natl Sci. Rev.* **2,** 140–149 (2015).
106. Doyle, A. D., Montoya, J. H. & Vojvodic, A. Improving oxygen electrochemistry through nanoscopic confinement. *ChemCatChem* **7,** 738–742 (2015).
107. Rosen, B. A. *et al.* Ionic liquid-mediated selective conversion of CO_2 to CO at low overpotentials. *Science* **334,** 643–644 (2011).
108. Thorson, M. R., Siil, K. I. & Kenis, P. J. A. Effect of cations on the electrochemical conversion of CO_2 to CO. *J. Electrochem. Soc.* **160,** F69–F74 (2012).
109. Sun, L., Ramesha, G. K., Kamat, P. V & Brennecke, J. F. Switching the reaction course of electrochemical CO_2 reduction with ionic liquids. *Langmuir* **30,** 6302–6308 (2014).
110. Chen, Y., Li, C. W. & Kanan, M. W. Aqueous CO_2 reduction at very low overpotential on oxide-derived Au nanoparticles. *J. Am. Chem. Soc.* **134,** 19969–19972 (2012).
111. Li, C. W., Ciston, J. & Kanan, M. W. Electroreduction of carbon monoxide to liquid fuel on oxide-derived nanocrystalline copper. *Nature* **508,** 504–507 (2014).
112. Feng, X., Jiang, K., Fan, S. & Kanan, M. W. Grain-boundary-dependent CO_2 electroreduction activity. *J. Am. Chem. Soc.* **137,** 4606–4609 (2015).
113. Norskov, J. K., Abild-Pedersen, F., Studt, F. & Bligaard, T. Density functional theory in surface chemistry and catalysis. *Proc. Natl Acad. Sci. USA* **108,** 937–943 (2011).
114. Michalsky, R., Zhang, Y.-J., Medford, A. J. & Peterson, A. A. Departures from the adsorption energy scaling relations for metal carbide catalysts. *J. Phys. Chem. C* **118,** 13026–13034 (2014).
115. Zhang, B. *et al.* Homogeneously dispersed, multimetal oxygen-evolving catalysts. *Science* **352,** 333–337 (2016).
116. Tripkovic, V. *et al.* Electrochemical CO_2 and CO reduction on metal-functionalized porphyrin-like graphene. *J. Phys. Chem. C* **117,** 9187–9195 (2013).
117. Fujishima, A. & Honda, K. Electrochemical photolysis of water at a semiconductor electrode. *Nature* **238,** 37–38 (1972).
118. Montoya, J. H., Garcia-Mota, M., Nørskov, J. K. & Vojvodic, A. Theoretical evaluation of the surface electrochemistry of perovskites with promising photon absorption properties for solar water splitting. *Phys. Chem. Chem. Phys.* **17,** 2634–2640 (2014).
119. Nielander, A. C., Shaner, M. R., Papadantonakis, K. M., Francis, S. A. & Lewis, N. S. A taxonomy for solar fuels generators. *Energy Environ. Sci.* **8,** 16–25 (2015).
120. Walter, M. G. *et al.* Solar water splitting cells. *Chem. Rev.* **110,** 6446–6473 (2010).
121. Guijarro, N., Prevot, M. S. & Sivula, K. Surface modification of semiconductor photoelectrodes. *Phys. Chem. Chem. Phys.* **17,** 15655–15674 (2015).
122. Nellist, M. R., Laskowski, F. A. L., Lin, F., Mills, T. J. & Boettcher, S. W. Semiconductor–electrocatalyst interfaces: theory, experiment, and applications in photoelectrochemical water splitting. *Acc. Chem. Res.* **49,** 733–740 (2016).
123. Seger, B. *et al.* Hydrogen production using a molybdenum sulfide catalyst on a titanium-protected n^+p-silicon photocathode. *Angew. Chem. Int. Ed.* **51,** 9128–9131 (2012).
124. Benck, J. D. *et al.* Designing active and stable silicon photocathodes for solar hydrogen production using molybdenum sulfide nanomaterials. *Adv. Energy Mater.* **4,** 1400739 (2014).
125. McKone, J. R. *et al.* Evaluation of Pt, Ni, and Ni-Mo electrocatalysts for hydrogen evolution on crystalline Si electrodes. *Energy Environ. Sci.* **4,** 3573–3583 (2011).

126. Kibsgaard, J., Jaramillo, T. F. & Besenbacher, F. Building an appropriate active-site motif into a hydrogen-evolution catalyst with thiomolybdate $[Mo_3S_{13}]^{2-}$ clusters. *Nat. Chem.* **6,** 248–253 (2014).
127. Peter, L. M. & Upul Wijayantha, K. G. Photoelectrochemical water splitting at semiconductor electrodes: fundamental problems and new perspectives. *ChemPhysChem* **15,** 1983–1995 (2014).
128. Sivula, K. Metal oxide photoelectrodes for solar fuel production, surface traps, and catalysis. *J. Phys. Chem. Lett.* **4,** 1624–1633 (2013).
129. Bard, A. J., Fan, F.-R. F., Gioda, A. S., Nagasubramanian, G. & White, H. S. On the role of surface states in semiconductor electrode photoelectrochemical cells. *Faraday Discuss. Chem. Soc.* **70,** 19–31 (1980).
130. Hamann, T. W. Splitting water with rust: hematite photoelectrochemistry. *Dalt. Trans.* **41,** 7830–7834 (2012).
131. Klahr, B., Gimenez, S., Fabregat-Santiago, F., Hamann, T. & Bisquert, J. Water oxidation at hematite photoelectrodes: the role of surface states. *J. Am. Chem. Soc.* **134,** 4294–4302 (2012).
132. Klahr, B., Gimenez, S., Fabregat-Santiago, F., Bisquert, J. & Hamann, T. W. Photoelectrochemical and impedance spectroscopic investigation of water oxidation with 'Co–Pi'-coated hematite electrodes. *J. Am. Chem. Soc.* **134,** 16693–16700 (2012).
133. Braun, A. *et al.* Direct observation of two electron holes in a hematite photoanode during photoelectrochemical water splitting. *J. Phys. Chem. C* **116,** 16870–16875 (2012).
134. Hisatomi, T. *et al.* Cathodic shift in onset potential of solar oxygen evolution on hematite by 13-group oxide overlayers. *Energy Environ. Sci.* **4,** 2512–2515 (2011).
135. Barroso, M. *et al.* Dynamics of photogenerated holes in surface modified α-Fe_2O_3 photoanodes for solar water splitting. *Proc. Natl Acad. Sci. USA* **109,** 15640–15645 (2012).
136. Gamelin, D. R. Water splitting: catalyst or spectator? *Nat. Chem.* **4,** 965–967 (2012).
137. Seabold, J. A. & Choi, K.-S. Efficient and stable photo-oxidation of water by a bismuth vanadate photoanode coupled with an iron oxyhydroxide oxygen evolution catalyst. *J. Am. Chem. Soc.* **134,** 2186–2192 (2012).
138. Kim, T. W. & Choi, K.-S. Nanoporous $BiVO_4$ photoanodes with dual-layer oxygen evolution catalysts for solar water splitting. *Science* **343,** 990–994 (2014).
139. Lin, F. & Boettcher, S. W. Adaptive semiconductor/electrocatalyst junctions in water-splitting photoanodes. *Nat. Mater.* **13,** 81–86 (2014).
140. Zhou, X. *et al.* Interface engineering of the photoelectrochemical performance of Ni-oxide-coated n-Si photoanodes by atomic-layer deposition of ultrathin films of cobalt oxide. *Energy Environ. Sci.* **8,** 2644–2649 (2015).
141. Hikita, Y. *et al.* Band edge engineering of oxide photoanodes for photoelectrochemical water splitting: integration of subsurface dipoles with atomic-scale control. *Adv. Energy Mater.* **6,** 1502154 (2016).
142. Hu, Y.-S., Kleiman-Shwarsctein, A., Stucky, G. D. & McFarland, E. W. Improved photoelectrochemical performance of Ti-doped α-Fe_2O_3 thin films by surface modification with fluoride. *Chem. Commun.* **2009,** 2652–2654 (2009).
143. Hunger, R. *et al.* Chemical and electronic characterization of methyl-terminated Si(111) surfaces by high-resolution synchrotron photoelectron spectroscopy. *Phys. Rev. B* **72,** 045317 (2005).
144. Chen, Y. W. *et al.* Atomic layer-deposited tunnel oxide stabilizes silicon photoanodes for water oxidation. *Nat. Mater.* **10,** 539–544 (2011).
145. Pourbaix, M. *Atlas of Electrochemical Equilibria in Aqueous Solutions* (Pergamon, 1966).
146. Mei, B. *et al.* Crystalline TiO_2: a generic and effective electron-conducting protection layer for photoanodes and -cathodes. *J. Phys. Chem. C* **119,** 15019–15027 (2015).
147. Sun, K. *et al.* Stable solar-driven oxidation of water by semiconducting photoanodes protected by transparent catalytic nickel oxide films. *Proc. Natl Acad. Sci. USA* **112,** 3612–3617 (2015).
148. Mei, B. *et al.* Iron-treated NiO as a highly transparent p-type protection layer for efficient Si-based photoanodes. *J. Phys. Chem. Lett.* **5,** 3456–3461 (2014).
149. Shaner, M. R., Hu, S., Sun, K. & Lewis, N. S. Stabilization of Si microwire arrays for solar-driven H_2O oxidation to O_2(g) in 1.0 M KOH(aq) using conformal coatings of amorphous TiO_2. *Energy Environ. Sci.* **8,** 203–207 (2015).
150. Ping, Y., Goddard, W. A. & Galli, G. A. Energetics and solvation effects at the photoanode/catalyst interface: ohmic contact versus Schottky barrier. *J. Am. Chem. Soc.* **137,** 5264–5267 (2015).
151. Matsubu, J. C. *et al.* Critical role of interfacial effects on the reactivity of semiconductor–cocatalyst junctions for photocatalytic oxygen evolution from water. *Catal. Sci. Technol.* **6,** 6836–6844 (2016).
152. Walczak, K. *et al.* Modeling, simulation, and fabrication of a fully integrated, acid-stable, scalable solar-driven water-splitting system. *ChemSusChem* **8,** 544–551 (2015).
153. Popczun, E. J., Read, C. G., Roske, C. W., Lewis, N. S. & Schaak, R. E. Highly active electrocatalysis of the hydrogen evolution reaction by cobalt phosphide nanoparticles. *Angew. Chem. Int. Ed.* **126,** 5531–5534 (2014).

Acknowledgements

The OER, ORR and HER work was supported by the US DOE, Office of Science, Basic Energy Sciences, Chemical Sciences, Geosciences and Bio Sciences Division through the SUNCAT Center for Interface Science. The work on CO_2 reduction was supported by the Joint Center for Artificial Photosynthesis, a DOE Energy Innovation Hub, supported through the Office of Science of the US DOE under Award Number DE-SC0004993. Helpful discussions and insights from Jakob Kibsgaard and Thomas Hellstern are also gratefully acknowledged.

Additional information

Reprints and permissions information is available online at www.nature.com/reprints. Correspondence should be addressed to J.K.N.

Competing financial interests

The authors declare no competing financial interests.